

## Overcoming the Diffraction Limit Using Multiple Light Scattering in a Highly Disordered Medium

Youngwoon Choi,<sup>1</sup> Taeseok Daniel Yang,<sup>1</sup> Christopher Fang-Yen,<sup>2</sup> Pilsung Kang,<sup>1</sup> Kyoung Jin Lee,<sup>1</sup> Ramachandra R. Dasari,<sup>3</sup> Michael S. Feld,<sup>3</sup> and Wonshik Choi<sup>1,\*</sup>

<sup>1</sup>*Department of Physics, Korea University, Seoul 136-701, Korea*

<sup>2</sup>*Department of Bioengineering, University of Pennsylvania, Philadelphia, Pennsylvania 19104, USA*

<sup>3</sup>*G. R. Harrison Spectroscopy Laboratory, Massachusetts Institute of Technology, Cambridge, Massachusetts 02139, USA*

(Received 27 February 2011; revised manuscript received 26 April 2011; published 6 July 2011)

We report that disordered media made of randomly distributed nanoparticles can be used to overcome the diffraction limit of a conventional imaging system. By developing a method to extract the original image information from the multiple scattering induced by the turbid media, we dramatically increase a numerical aperture of the imaging system. As a result, the resolution is enhanced by more than 5 times over the diffraction limit, and the field of view is extended over the physical area of the camera. Our technique lays the foundation to use a turbid medium as a far-field superlens.

DOI: 10.1103/PhysRevLett.107.023902

PACS numbers: 42.25.Dd, 05.60.-k, 73.23.-b

A conventional lens performs imaging by focusing waves scattered from an object onto a detector [Fig. 1(a)]. The most oblique angle,  $\theta_{\max}$ , that the lens can capture sets the diffraction-limit resolution, which is given by  $1.22\lambda/\text{N.A.}$ , where  $\lambda$  is the wavelength of the source and  $\text{N.A.} = n \sin\theta_{\max}$  with  $n$  the index of refraction of the medium [1]. If a turbid medium with a highly disordered internal structure is placed between the object and the lens [Fig. 1(b)], the direction and positions of rays from the object are essentially randomized due to scattering in the medium. Consequently, the object image becomes highly deteriorated or disappears entirely.

In the past decades, many schemes have been introduced to cancel the image deterioration caused by turbidity. They have used either statistical correction of diffusing photons [2,3] or active control of the wave front in order to mitigate the effect of turbidity [4–6]. However, the disordered medium is not necessarily a barrier to overcome. The disordered medium can capture evanescent waves and convert them into far-field propagating waves. Recent studies in microwave and ultrasound have achieved sub-wavelength focusing by using time reversal mirrors to reverse the far-field waves into evanescent waves [7,8]. In optics, feedback control has been used to optimize a transmitted wave through a disordered medium to a spot of improved sharpness [9], and the spot is scanned to perform an imaging [10,11]. But the application of time reversal mirror and feedback control processes are both limited to the scanning microscopy, and the use of a turbid medium to overcome the diffraction limit in wide-field imaging has not yet been explored.

In this Letter, we present a method that converts a turbid medium into a lens. We call this method turbid lens imaging (TLI) and demonstrate that the turbid lens can perform wide-area imaging, rather than focusing a beam, with dramatically improved spatial resolution and an enlarged

field of view of an imaging system. As illustrated in Fig. 1(b), a wave scattered at an angle  $\theta_T$  greater than  $\theta_{\max}$  can be redirected into the camera by multiple scattering in the medium. For any incoming waves, the disordered medium diverts outgoing waves over the entire solid angle so that a lens with a small N.A. can capture high-angle scattered waves from the object. Therefore, the insertion of the turbid medium can potentially break the diffraction limit of a conventional lens provided that the captured waves are appropriately processed to extract image information.

The randomness of a disordered medium can also dramatically influence another fundamental parameter of imaging: the field of view. In conventional imaging the size

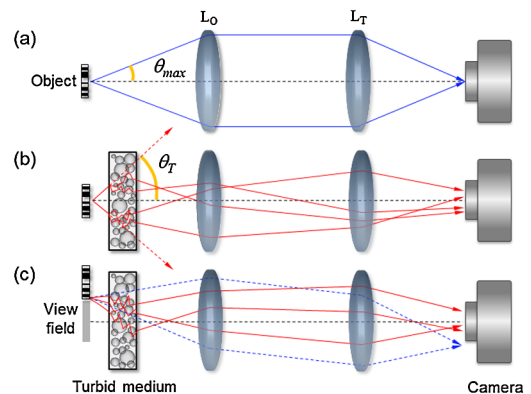


FIG. 1 (color online). Experimental schematics. (a) Conventional imaging with an objective ( $L_O$ ) and a tube ( $L_T$ ) lenses.  $\theta_{\max}$  is the maximum angle that the object lens can accept. (b) Scattered wave whose angle  $\theta_T$  exceeding  $\theta_{\max}$  can be captured after inserting a disordered medium. (c) The scattered waves reach the camera sensor through multiple scattering process (solid red lines), although the object is shifted away from the conventional field of view (gray area).

of the field of view is given by  $L/M$ , where  $L$  is the size of the image sensor and  $M$  is the magnification of the imaging system. However, the insertion of the disordered medium can increase the imaging area over the limit set by this relation. As shown in Fig. 1(c), a scattered wave at a point in an object located outside the field of view does not reach the camera sensor in ordinary imaging (dashed blue lines). But when a turbid medium is introduced, it redirects some of the transmitted waves to the camera sensor via multiple scattering. Therefore, the disordered medium allows the collection of light from an object located outside the conventional field of view.

A key challenge in taking advantage of the two unique benefits of the turbidity—breaking the diffraction barrier and enlargement of the field of view—is to extract the image information from the multiply scattered waves. Consider the scattered waves emerging from an object in Fig. 1(b). When they propagate through the disordered medium, they are spatially mixed and become almost indistinguishable at the camera plane. However, the object information is not lost but rather scrambled. Here we introduce a method to retrieve an object image out of the scrambled one. First, we characterize the input-output response of a turbid medium by the so-called transmission matrix, and we compare the object image scrambled by the turbid medium with the transmission matrix. By calculating the correlation between the transmission matrix and the distorted image, we can recover the object image at the input side of the disordered medium from the distorted image at the output side.

To record the transmission matrix of a disordered medium, we illuminate the medium with a laser beam and record the output images,  $E_{\text{trans}}(x, y; \theta_x, \theta_y)$ , while scanning the angle of illumination  $(\theta_x, \theta_y)$  [Fig. 2(a)]. Figure 2(b) shows a set of the output images taken for a disordered medium, a  $25 \mu\text{m}$  thick layer of ZnO nanoparticles ( $T = 6\%$  average transmission). For this recording, we used a tomographic phase microscopy [12], a high speed interferometric microscopy system equipped with a speckle-field imaging ability [3,4]. It rapidly scans the illumination and records the electric field image, not the intensity image, of the output waves by digital holography [5] (see [13]). It takes 40 s to record 20 000 images covering the angular range of illumination corresponding to 0.5 N.A. A set of output images forms a base set that makes the deterministic connection between the input and output of the disordered medium. Once this transmission matrix has been determined, the disordered medium is no longer an obstacle to imaging but instead can act as an unconventional lens with interesting properties.

We demonstrate TLI for a resolution target pattern [Fig. 2(f)] located at the sample plane [Fig. 2(c)]. The object scatters an incoming beam into multiple angular waves. Each angular wave becomes distorted in its own way independent of the others and is linearly superposed with the others to form a distorted image of the object,  $E_d(x, y)$  [Fig. 2(d)]. Through a projection operation

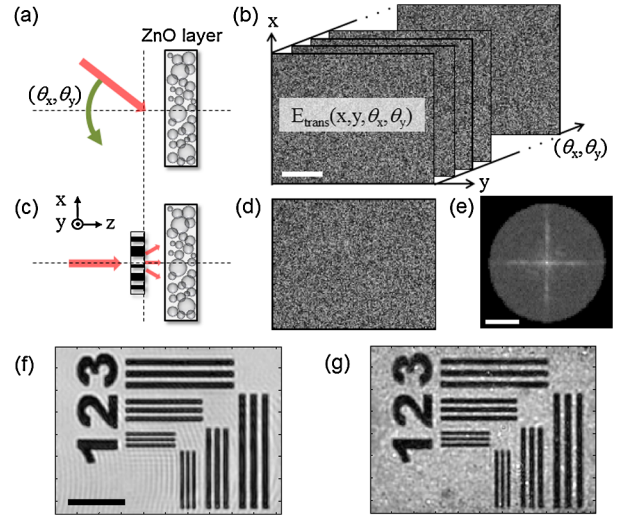


FIG. 2 (color online). Schematics of TLI. (a) Recording of the transmission matrix for a disordered medium. The incident angle of a plane wave,  $(\theta_x, \theta_y)$ , from a He-Ne laser ( $\lambda = 633 \text{ nm}$ ) is scanned, and the transmitted wave is recorded at each incident angle. (b) The recorded transmission images constituting a transmission matrix. Only amplitude images are shown here, although conjugate phase images are recorded at the same time. (c) Recording of an object image following the configuration of Fig. 1(b). (d) The distorted image of an object, a resolution target pattern. (e) Angular spectrum of the object acquired by projection operation (see the text). Only amplitude components are shown here, although the phase information is also crucial (see [13]). Scale bar:  $0.5 \mu\text{m}^{-1}$ . (f) The resolution target image taken prior to inserting the ZnO layer. Scale bar:  $10 \mu\text{m}$ . (g) The target image reconstructed from the angular spectrum in (e).

between each angular component of the transmission matrix  $E_{\text{trans}}(x, y; \theta_x, \theta_y)$  and the distorted image of the object, we retrieve the spectrum of angular waves,  $A(\theta_x, \theta_y)$ , constituting the object image:

$$A(\theta_x, \theta_y) = \sum_{x,y} E_{\text{trans}}^*(x, y; \theta_x, \theta_y) E_d(x, y). \quad (1)$$

It should be noted that the angular extent of the angular spectrum corresponds to that of the recorded transmission matrix. Figure 2(e) shows the angular spectrum acquired from the distorted image of an object, and the reconstructed image from this angular spectrum [Fig. 2(g)] shows an excellent structural correspondence with the original object. This clearly proves that TLI unscrambles the effect of multiple scatterings.

In contrast to previous transmission matrix approaches that recorded transmission images with respect to a self-referenced speckle wave [14], TLI measures the real transmission matrix of a disordered medium due to the use of a clean reference wave with a unique phase referencing method. It is thus possible to image a real object through a disordered medium instead of virtual objects. To clearly demonstrate this ability, we perform imaging of a live biological cell through a tissue slice of  $450 \mu\text{m}$  thickness (see [13]).

We now demonstrate a spatial resolution enhancement using a disordered medium. A barodelike pattern is used as a target object, and its image is taken at first by a high N.A. objective lens (1.0 N.A.) in a conventional imaging configuration [Fig. 3(a)]. The finest lines bounded by the red box are well resolved because their spatial period,  $2.5 \mu\text{m}$ , is larger than the diffraction limit ( $0.77 \mu\text{m}$ ). The spectrum of the finest lines reveals a peak conjugate to the periodicity [an orange arrow indicated at the blue curve in Fig. 3(e)]. We then take an image of the same object with a low N.A. objective lens (0.15 N.A.) [Fig. 3(b)]. The finest pattern is indistinguishable due to insufficient resolving power. Some other fine structures marked as red arrows are also invisible for the same reason. In the spectrum of the finest lines, the peak associated with the structure disappears [green curve in Fig. 3(e)]. Then we place ZnO nanoparticle layers as a disordered medium between the low N.A. lens and the object following the configuration in Fig. 1(b). First, we record the transmission matrix of the ZnO layers. Despite the fact that the objective lens N.A. is limited to 0.15, the transmission matrix can be recorded up to 0.85 N.A. (see [13] for the recorded transmission matrix) because the disordered medium converts a high-angle component to a low-angle one. If the ZnO layers were not inserted, the transmission

matrix would be limited to an angular extent corresponding to 0.15 N.A. Next, the object image distorted by the ZnO layers is taken: This image exhibits a speckle pattern with an average speckle size corresponding to the diffraction limit set by 0.15 N.A. [Fig. 3(c)]. However, it contains high-angle scattered waves as well as low-angle ones. Using projection operation, we extract the angular spectrum of the object,  $A(\theta_x, \theta_y)$ , embedded in the distorted image, and from  $A(\theta_x, \theta_y)$  we reconstruct the object image [Fig. 3(d)]. The finest lines are well resolved with a spectrum exhibiting an associated peak [orange arrow over the red curve in Fig. 3(f)].

In recording the transmission matrix, we scan the angle of the input wave from  $-53^\circ$  to  $53^\circ$  (0.85 N.A.) in 5000 steps along the direction orthogonal to the barodelike lines in the object. Thus we obtain the object spectrum from the distorted image up to 0.85 N.A., not the 0.15 N.A. The numerical aperture is increased by more than fivefold, and the spatial resolution increases by the same factor. It should be noted that the 0.85 N.A. is not a fundamental limit. A random medium can capture any input wave, even evanescent waves, as long as the particles constituting the medium are smaller than the wavelength [8].

Turbidity is related to the fidelity of imaging in TLI. In our study, we vary the thickness of ZnO layers and use their average transmission as a criterion of turbidity: The lower the transmission, the higher the turbidity of the medium. As the turbidity increases, the ability of a disordered medium to convert high-angle input waves to low angles of output is increased. Specifically, the peak indicated by an orange arrow in Fig. 3(f) represents a scattered wave from the object with an angle of  $27^\circ$  captured by a 0.15 N.A. objective lens (maximum acceptance angle:  $9^\circ$ ), which is the result of the disordered medium deflecting the angle of an incoming wave. When a turbid medium with an average transmission coefficient of 70% is used instead of 6%, its angular conversion efficiency is lower than the previous one. As a result, the peak at the spectrum [black curve in Fig. 3(f)] is attenuated due to the reduced turbidity. For turbid media of various average transmissions, we obtain the signal to noise ratio, which is the peak height divided by the baseline noise of the spectrum, and normalize it with that of the high N.A. object image [Fig. 3(g)]. As the turbidity decreases, the signal to noise ratio drops and noise in the reconstructed image is increased. This result shows clearly that high turbidity is favorable for TLI.

The second benefit of turbidity is the enlargement of the field of view. As mentioned earlier, the wave scattered from an object located outside of the field of view can be scattered into the camera sensor by a disordered medium [Fig. 1(c)]. This results in an interesting phenomenon: Even though we do not directly image an object, the object can be imaged by using the scattered light. To demonstrate this concept, we prepare an object with a blank upper part and a periodic pattern in its bottom part [Fig. 4(a)]. With ZnO layers in place, we obtain a highly distorted image as shown in Fig. 4(b). We narrow our view field only to the

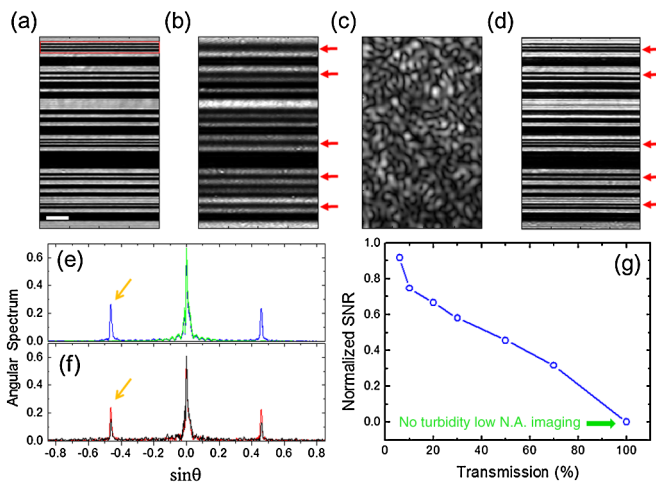


FIG. 3 (color online). TLI overcomes the diffraction limit. (a) A conventional imaging by a high N.A. objective lens (1.0 N.A.) and (b) by a low N.A. objective lens (0.15 N.A.), respectively. The fine pitches indicated by red arrows are not visible in (b). Scale bar:  $10 \mu\text{m}$ . (c) A distorted image of the object taken by a low N.A. objective lens after inserting ZnO layers ( $T = 6\%$ ). (d) Object image recovered from the distorted image in (c) by TLI. Fine pitches are visible even if the image is taken by a 0.15 N.A. objective lens. (e) Angular spectra from the finest lines [red box in (a)] taken by high N.A. (blue curve) and low N.A. (green curve) objective lenses, respectively. The peak indicated by an orange arrow is conjugate to the periodicity of the structure. (f) The angular spectra acquired from the distorted image for turbid media of high turbidity ( $T = 6\%$ , red curve) and low turbidity ( $T = 70\%$ , black curve), respectively. (g) Normalized signal to noise ratio defined in the text is plotted for various turbid media.

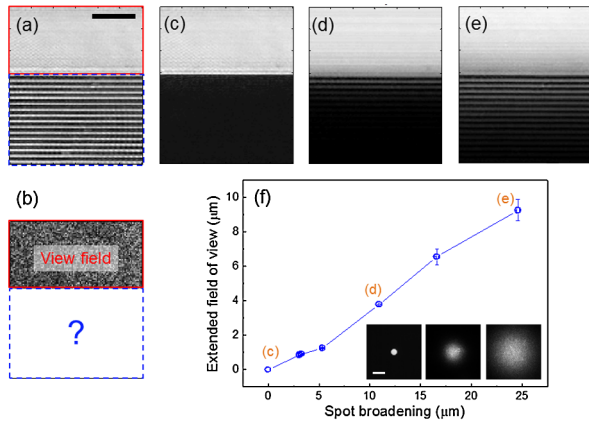


FIG. 4 (color online). Field of view enlargement by TLI. (a) A target object without turbidity and (b) with turbidity. Only the solid red box is a recording area. Scale bar:  $10 \mu\text{m}$ . (c)–(e) Reconstructed images under various turbidities of  $T = 100\%$  [(c), no turbidity],  $T = 20\%$  (d), and  $T = 6\%$  (e). (f) The extended field of view versus the spot broadening for various turbidities. The extended field of view is estimated to the extent that the contrast of structure drops by one half. The HWHM of the transmitted image of a spot ( $5 \mu\text{m}$  in diameter) through a disordered medium is used to determine the spot broadening. Representative broadened spot images are shown at the bottom of the figure. From left,  $T = 100\%$ ,  $20\%$ , and  $6\%$ , respectively. Scale bar:  $10 \mu\text{m}$ . Data points correspond to the transmission of  $T = 100\%$ ,  $70\%$ ,  $50\%$ ,  $30\%$ ,  $20\%$ ,  $10\%$ , and  $6\%$ , reading, respectively, from the left.

upper part (solid red box) for recording both the distorted sample image and the transmission matrix of the disordered medium. When there is no turbid medium ( $T = 100\%$ ), the image in the solid red box contains no information on the object, leaving the image in the dashed blue box invisible [Fig. 4(c)]. By contrast, when ZnO layers are inserted, we can reconstruct the object image in the dashed blue box with the data acquired in the solid red box [Figs. 4(d) and 4(e)]. As the transmission becomes lower from  $20\%$  [Fig. 4(d)] to  $6\%$  [Fig. 4(e)], the range over which the image can be reconstructed is extended beyond the normal field of view. This observation agrees well with the tendency of the image of a spot to spread laterally during transmission through disordered media [Fig. 4(f)].

In conclusion, we have demonstrated that turbidity both improves the spatial resolution of an objective lens beyond its diffraction limit and extends its field of view. These two improvements result from the angular and spatial spread of light by multiple scatterings in a disordered medium. The development of TLI to exploit multiple scattering allows a turbid medium to become a unique lens with counterintuitive imaging properties. This work is an important step beyond previous studies that used a turbid medium to achieve subdiffraction focusing in ultrasound and optics and near-field focusing with microwaves [7–9]. Our work uses turbid media to achieve subdiffraction imaging, not focusing. We open a way to convert a random medium into a superlens with no need of any metamaterial by using the

fact that disordered media with structures finer than a wavelength can capture evanescent waves [15,16]. Our approach can also serve as a way to find the open channels of disordered media, those with transmission close to  $100\%$  [17]. These provide the prospect of potential applications for random lasers [18]. In addition to imaging applications, TLI can also be applied to cryptography by generating a copyproof random medium to protect a pass code [19].

We thank Charles H. Holbrow for valuable advice and discussions. This research was supported by Basic Science Research Program through National Research Foundation of Korea (NRF) funded by the Ministry of Education, Science and Technology (2011-0005018 and 2011-0016568), National R&D Program for Cancer Control, Ministry of Health & Welfare, Republic of Korea (1120290), KOSEF (R17-2007-017-01000-0), Korea University grant, and the National Institutes of Health (P41-RR02594-24).

\*wonsnik@korea.ac.kr

- [1] M. Born, E. Wolf, and A. B. Bhatia, *Principles of Optics: Electromagnetic Theory of Propagation, Interference and Diffraction of Light* (Cambridge University Press, Cambridge, England, 1999), 7th ed.
- [2] J. Wu, L. Perelman, R. R. Dasari, and M. S. Feld, *Proc. Natl. Acad. Sci. U.S.A.* **94**, 8783 (1997).
- [3] M. J. Niedre *et al.*, *Proc. Natl. Acad. Sci. U.S.A.* **105**, 19 126 (2008).
- [4] H. W. Babcock, *Science* **249**, 253 (1990).
- [5] N. Ji, D. E. Milkie, and E. Betzig, *Nat. Methods* **7**, 141 (2009).
- [6] Z. Yaqoob, D. Psaltis, M. S. Feld, and C. Yang, *Nat. Photon.* **2**, 110 (2008).
- [7] A. Derode, P. Roux, and M. Fink, *Phys. Rev. Lett.* **75**, 4206 (1995).
- [8] G. Lerosey, J. De Rosny, A. Tourin, and M. Fink, *Science* **315**, 1120 (2007).
- [9] I. M. Vellekoop, A. Lagendijk, and A. P. Mosk, *Nat. Photon.* **4**, 320 (2010).
- [10] I. M. Vellekoop and C. M. Aegerter, *Opt. Lett.* **35**, 1245 (2010).
- [11] E. G. van Putten *et al.*, *Phys. Rev. Lett.* **106**, 193905 (2011).
- [12] W. Choi *et al.*, *Nat. Methods* **4**, 717 (2007).
- [13] See supplemental material at <http://link.aps.org/supplemental/10.1103/PhysRevLett.107.023902> for detailed experimental setup, data processing methods, and sample preparation.
- [14] S. M. Popoff *et al.*, *Phys. Rev. Lett.* **104**, 100601 (2010).
- [15] N. Fang, H. Lee, C. Sun, and X. Zhang, *Science* **308**, 534 (2005).
- [16] T. Taubner *et al.*, *Science* **313**, 1595 (2006).
- [17] I. M. Vellekoop and A. P. Mosk, *Phys. Rev. Lett.* **101**, 120601 (2008).
- [18] J. Fallert *et al.*, *Nat. Photon.* **3**, 279 (2009).
- [19] R. Pappu, R. Recht, J. Taylor, and N. Gershenfeld, *Science* **297**, 2026 (2002).